Geophys. J. Int. (2000) **140,** 385–398

On galvanic distortion of regional three-dimensional magnetotelluric impedances

Hisashi Utada and Hiroshi Munekane

Earthquake Research Institute, University of Tokyo, 1-1-1 *Yayoi, Bunkyo-ku Tokyo,* 113-0032, *Japan. E-mail: utada@utada-sun.eri.u-tokyo.ac.jp*

Accepted 1999 September 10. Received 1999 September 7; in original form 1998 October 12

SUMMARY

In magnetotelluric (MT) studies, the observed response function (the MT impedance) usually suffers from galvanic distortions due to near-surface inhomogeneities. Removal of these effects is essential to obtain an accurate model of the subsurface electrical conductivity structure. Galvanic distortion is usually expressed by a simple real tensor multiplying the undistorted regional impedance. The problem still remains of how to solve the ensuing linear equations in order to determine the distortion tensor and then to obtain the undistorted impedance. The methods presented and widely applied in previous works assume two-dimensionality for the undistorted impedance. This paper proposes a method that employs a relationship between the spatial derivatives of the horizontal electric field and the vertical geomagnetic component, which can be directly derived from Faraday's law. The identity derived from the relationship is written using the vertical magnetic transfer function, the impedance, and the spatial derivatives of the impedance and horizontal magnetic transfer functions. The present method determines the real distortion tensor so that the identity is satisfied. Therefore, the method has two major advantages: (1) galvanic distortion that is to be removed from the impedance tensor is clearly defined, and (2) the method is applicable even when the regional structure is 3-D.

Key words: Faraday's law, galvanic distortion, geomagnetic transfer functions, induction effects, MT impedance, tensor decomposition.

INTRODUCTION

The magnetotelluric (MT) method is widely used to explore electrical conductivity structures on both local and regional scales. In recent years, remarkable progress has been made in instrumentation, data processing and data interpretation schemes. In interpreting the observed response functions (the impedance tensor) in terms of the conductivity distribution of the Earth, 2-D inversion schemes have been widely and successfully applied (e.g. Pedersen & Rasmussen 1985; Smith & Booker 1991; Uchida 1993). In order to obtain a reliable model reflecting the regional resistivity structure, it is usually necessary to separate the effect of galvanic distortion from the observed impedance tensor.

Galvanic distortion can be recognized as a superposition of regional and locally distorted electromagnetic (EM) fields (Groom & Bahr 1992). Regional EM fields are thought simply to reflect the background regional structure that is either 1-D or 2-D, while distorted fields are assumed to be due to non-inductive (galvanic) scattering by local, near-surface inhomogeneities. Assuming that this is the situation, several methods have been presented to recover 1-D or 2-D responses from the observed impedance tensor.

Bahr (1988) first described the electric field distortion due to 3-D local heterogeneity in a 2-D regional structure, and applied the method to discriminate the distortion effects from field data. Meanwhile, Groom & Bailey (1989) derived a physical parametrization of the electric distortion tensor and developed a scheme to decompose the observed impedance tensor into distortion parameters and undistorted MT responses. This approach, hereafter referred to as GB decomposition, is the most widely used for interpreting magnetotelluric data. In recent years, the GB decomposition method has been regarded as part of the common procedure for obtaining a highly objective 2-D resistivity model combined with sophisticated 2-D inversion schemes (e.g. Ogawa & Uchida 1996).

However, a 2-D conductivity model can only approximate the actual 3-D structure of the Earth. It is not uncommon that 3-D effects, not only of local scale but also of regional scale, are too strong to be ignored. Meanwhile, rapid progress in numerical modelling schemes has made it quite feasible to interpret the field MT data for 3-D structures either by forward modelling or by inversion (e.g. Mackie *et al.* 1993; Zhdanov & Fang 1996; Avdeev *et al.* 1997). To estimate the correct 3-D structure, regional MT response functions are needed. In other words, galvanic distortions must be removed from the

observed raw MT response to extract the undistorted part that is reflecting the 3-D regional structure.

This paper aims to re-examine and clarify the physics of galvanic distortion when the background regional structure is 3-D and to propose a new mathematical condition to determine the distortion parameters by using not only the observed impedance tensor but also the observed geomagnetic transfer functions. Zhang *et al.* (1993) also proposed a method to separate galvanic distortion effects from those of induction by using vertical magnetic field data, but a different approach will be taken here.

DISTORTION MODEL

Fig. 1 provides a model of the galvanic distortion considered in this paper. The earth is composed of a 3-D large-scale heterogeneous structure covered by a near-surface thin layer with a plane interface consisting of smaller-scale 3-D inhomogeneities. Since both structure size and layer thickness should be scaled by the inductive scale length when considering electromagnetic induction, the actual size of a 'large' heterogeneity or actual thickness of a 'thin' layer depends on the frequency of interest (Zhang *et al.* 1993). In the following discussion, each expression is derived in the frequency domain at a frequency ω, but the frequency dependence of each parameter is not explicitly written in each equation.

Three-element vectors of the electromagnetic fields are denoted by bold type. In the MT method, vectors having only the two horizontal components often appear in governing equations. In this paper, the partitioned horizontal components of a three-element vector $\mathbf{u}_S$ are written as $\mathbf{u}_{\mathrm{h}}^S$, i.e.

$$\mathbf{u}_S = \begin{pmatrix} u_x^S \\ u_y^S \\ u_z^S \end{pmatrix} = \begin{pmatrix} \mathbf{u}_{\mathrm{h}}^S \\ \cdots \\ u_z^S \end{pmatrix} .$$

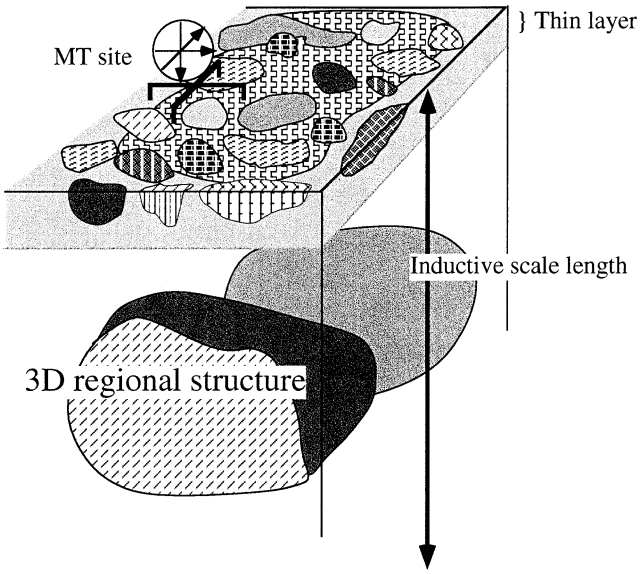

Figure 1. A model of the galvanic distortion considered in this paper. The Earth's electrical structure consists of 3-D heterogeneities of regional scale (comparable with the inductive scale length of present interest). The surface consists of a 3-D heterogeneous thin layer that causes galvanic distortion.

A mathematical expression is employed that describes galvanic distortion by a second-order tensor (e.g. Groom & Bailey 1989; Groom & Bahr 1992; Chave & Smith 1994). Namely, the distorted impedance $Z_{\mathrm{D}}(\mathbf{r})$ observed at site $\mathbf{r}$ is assumed to be described by

$$Z_{\mathrm{D}}(\mathbf{r}) = C(\mathbf{r}) Z_{\mathrm{U}}(\mathbf{r}) , \tag{1}$$

where $Z_{\mathrm{U}}(\mathbf{r})$ is the regional undistorted impedance tensor and $C(\mathbf{r})$ is the distortion tensor. This corresponds to the case in which the magnetic distortion terms are weak, as in the case studied by Groom & Bailey (1989).

Although the distortion tensor C can be a complex quantity in general (Jiracek 1990), the following discussion with electromagnetic scattering theory will demonstrate that it can be treated as a real tensor. As shown in Chave & Smith (1994), the electric field $\mathbf{E}(\mathbf{r})$ at an arbitrary position $\mathbf{r}$ in a 3-D heterogeneous medium can be described by an integral equation as follows (Hohmann 1975):

$$\begin{aligned} \mathbf{E}(\mathbf{r}) &= \mathbf{E}_0(\mathbf{r}) - i\omega\mu_0 \sum_j \int_{V_j} dV' \mathrm{g}(\mathbf{r}, \mathbf{r}') \delta\sigma_j(\mathbf{r}') \mathbf{E}(\mathbf{r}') \\ &\quad + \nabla \frac{1}{\sigma_0} \nabla \cdot \sum_j \int_{V_j} dV' [\mathrm{g}(\mathbf{r}, \mathbf{r}') \delta\sigma_j(\mathbf{r}') \mathbf{E}(\mathbf{r}')] \\ &= \mathbf{E}_0(\mathbf{r}) + \mathbf{e}_{\mathrm{I}}(\mathbf{r}) + \mathbf{e}_{\mathrm{G}}(\mathbf{r}) , \end{aligned} \tag{2}$$

where V_j refers to each scattering body, and μ_0 denotes the magnetic permeability. The conductivity anomaly $\delta\sigma_j(\mathbf{r}')$ is expressed by

$$\delta\sigma_j(\mathbf{r}') = \sigma_j(\mathbf{r}') - \sigma_0(\mathbf{r}') , \tag{3}$$

where σ_j is the heterogeneous conductivity distribution and σ_0 denotes either a uniform background or a background with a 1-D conductivity distribution for which an analytic expression of the Green function $\mathrm{g}(\mathbf{r}, \mathbf{r}')$ is available. The scalar uniform whole-space Green function is given by

$$\mathrm{g}(\mathbf{r}, \mathbf{r}') = \frac{\mathrm{e}^{(i\gamma_0 |\mathbf{r} - \mathbf{r}'|)}}{4\pi |\mathbf{r} - \mathbf{r}'|} , \tag{4}$$

where $\gamma_0 = \sqrt{i\omega\mu_0\sigma_0}$, and the inductive scale length of the background is defined as

$$\lambda_0 = \frac{1}{|\mathscr{R}e[\gamma_0]|} . \tag{5}$$

The first term of (2) corresponds to the field for the background structure, while the second and third terms are the inductive and galvanic scattered components due to each inhomogeneity, respectively. A similar integral expression for the magnetic field can be obtained by applying Faraday's law to (2):

$$\mathbf{B}(\mathbf{r}) = \mathbf{B}_0(\mathbf{r}) + \mu_0 \nabla \times \sum_j \int_{V_j} dV' \mathrm{g}(\mathbf{r}, \mathbf{r}') \delta\sigma_j(\mathbf{r}') \mathbf{E}(\mathbf{r}') , \tag{6}$$

in which the galvanic component does not show up because of the identity $\nabla \times \nabla\psi = 0$ for an arbitrary scalar function ψ.

Each scattered component contributes to the total field in a different way. From (2), the contribution of the inductive component from each body can be scaled by the ratio of the size, L_j, to the inductive scale length, $\lambda_j = 1/|\mathscr{R}e[\gamma_j]|$, where

$\gamma_j = \sqrt{i\omega\mu_0\delta\sigma_j}$. This ratio is called the induction number of each scattering body and may be expressed as

$$M_j = \left(\frac{L_j}{\lambda_j}\right). \tag{7}$$

When the scattering body is so small that the induction number M_j is substantially less than unity, the contribution due to the inductive scattered term may be neglected (Chave & Smith 1994; Smith 1997). For smaller L_j, the inductive scattered term in the electric field can be roughly estimated as $O(M_j^2)$, while that in the magnetic field can be estimated as $O(M_j)$ because of the rotation operator. On the other hand, the contribution of the galvanic scattered component from each scattering body does not depend greatly on M_j; rather, it depends on the distance from each body and the conductivity contrast (Groom & Bahr 1992). This is because the galvanic scattered field can be regarded as a potential field whose source is of delta function type due to the term $\delta\sigma(\mathbf{r}')$ in (2) (Jiracek 1990).

Using the scattering theory described above, we next examine the characteristics of the spatial distribution of scattered fields in the situation shown in Fig. 1. Because of the nature of the EM scattering, the scattered components in **E** and **B** have different dependences on the spatial wavenumber at a given frequency. The electric field is composed of small-wavenumber (long-wavelength) components due to large structures and large-wavenumber (short-wavelength) galvanic components originating from small-scale near-surface heterogeneities, while the magnetic field tends to contain the inductive scattered field components with smaller wavenumbers due to larger heterogeneities (Fig. 2). The large-wavenumber components

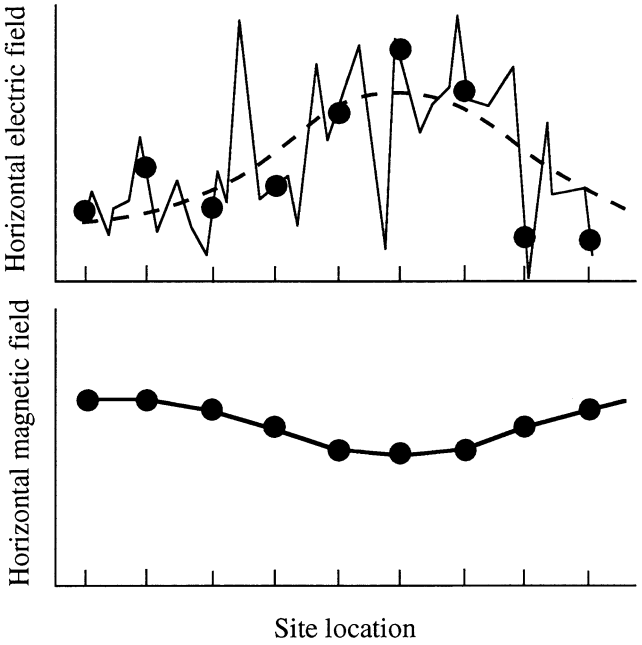

Figure 2. Typical spatial distribution of amplitudes of electromagnetic field variations. In the electric field (upper diagram), there exist components of shorter wavelengths (solid line) superimposed on the regional field with longer wavelength (dashed line) because of galvanic scattering. Such short-wavelength components barely exist in the magnetic field (thick line, lower diagram). In other words, the electric field is spatially aliased, whereas the magnetic field is not. This is a signature of galvanic distortion.

in the electric field will serve as 'noise' in the determination of regional conductivity structures. It is not impossible to describe all the spatial features of the field components and to remove the large-wavenumber terms from structures that are not of interest in the further interpretation by, for example, numerical modelling. However, it becomes impossible to describe such effects only by the observed data when site spacing is small enough to describe the scattered components due to the large structures but not small enough for the galvanic scattered components by near-surface small heterogeneities (Fig. 2), as is often the case in actual field surveys. This effect causes an error in MT data interpretation, which is called galvanic distortion. If the site spacing is too large to describe even the inductive scattered fields, the observed data set will contain not only galvanic distortion but also magnetic distortion (Chave & Smith 1994). In this case, however, the distortion tensor C can no longer be real due to the nature of the EM induction.

The galvanic distortion model considered here is caused purely by the galvanic scattered components in the electric field. The observed electric field **E** can be separated into regional undistorted (including inductively scattered components) and galvanic distorted components as follows:

$$\mathbf{E}(\mathbf{r}) = \mathbf{E}_{\mathrm{U}}(\mathbf{r}) + \mathbf{e}_{\mathrm{G}}(\mathbf{r}), \tag{8}$$

where $\mathbf{E}_{\mathrm{U}} = \mathbf{E}_0 + \mathbf{e}_{\mathrm{I}}$. When the size of each scattering body in the inhomogeneous thin layer is sufficiently small that the electric field inside can be regarded as uniform, the horizontal vector of the galvanic scattered field $\mathbf{e}_{\mathrm{h}}^{\mathrm{G}}$ can be related to the undistorted horizontal electric field $\mathbf{E}_{\mathrm{h}}^{\mathrm{U}}$ as follows:

$$\mathbf{e}_{\mathrm{h}}^{\mathrm{G}}(\mathbf{r}) = \alpha\mathbf{E}_{\mathrm{h}}^{\mathrm{U}}(\mathbf{r}), \tag{9}$$

where α is a second-order real tensor (Chave & Smith 1994; Smith 1995).

Comparing this with an expression of the impedance tensor of (1), we obtain the simple relation

$$C = I + \alpha, \tag{10}$$

where I is the second-order identity tensor. Thus, the distortion model described above justifies a simple treatment of the distortion tensor as a second-order real tensor.

CONSTRAINTS BY FARADAY'S LAW

In order to decompose the observed MT impedance into galvanic distortion and the undistorted impedance shown in (1), some constraints must be imposed to reduce the degrees of freedom to solve the equation for C (Groom & Bahr 1992; Smith 1995). The approach of Bahr (1988) or GB employed the constraint that the undistorted impedance is a 2-D response. However, in order to extract the 3-D regional undistorted impedance, another independent mathematical constraint is necessary. In this study, we propose a constraint that not only allows for a 3-D undistorted MT response but also is physically plausible by returning to the fundamentals of EM induction.

MT observations are used to obtain frequency characteristics and spatial distributions of three components of the magnetic field and two horizontal components of the electric field. These field components should satisfy the pre-Maxwell

equations

$$\nabla \times \mathbf{E} = -i\omega \mathbf{B}, \tag{11}$$

$$\nabla \times \mathbf{H} = \mathbf{j}, \tag{12}$$

in which $\mathbf{j}$ denotes the ohmic current, and the displacement current is ignored. However, even an ideal observation with site spacing small enough to evaluate the field gradients by finite differences accurately cannot fully describe all six components of (11) and (12), because vertical gradients are not usually measurable. Practically, only the vertical component of Faraday's law (11) can be fully described by the observed field components.

The vertical component of (11) can be written as

$$\nabla \times \mathbf{E}(\mathbf{r})|_z = \nabla \times \begin{pmatrix} \mathbf{E}_h(\mathbf{r}) \\ \cdots \\ E_z(\mathbf{r}) \end{pmatrix}\Bigg|_z = -i\omega\mu_0 H_z(\mathbf{r}). \tag{13}$$

The horizontal electric field $\mathbf{E}_h$ and vertical magnetic field component H_z at each observation site $\mathbf{r}$ can be expressed in terms of the impedance and vertical geomagnetic transfer function relations with the horizontal magnetic field $\mathbf{H}_h(\mathbf{r})$ as

$$\begin{aligned} \mathbf{E}_h(\mathbf{r}) &= Z(\mathbf{r})\mathbf{H}_h(\mathbf{r}) \\ &= \begin{pmatrix} Z_{xx}(\mathbf{r}) & Z_{xy}(\mathbf{r}) \\ Z_{yx}(\mathbf{r}) & Z_{yy}(\mathbf{r}) \end{pmatrix} \begin{pmatrix} H_x(\mathbf{r}) \\ H_y(\mathbf{r}) \end{pmatrix} \end{aligned} \tag{14}$$

and

$$H_z(\mathbf{r}) = \mathbf{T}_h(\mathbf{r}) \cdot \mathbf{H}_h(\mathbf{r}) = A(\mathbf{r})H_x(\mathbf{r}) + B(\mathbf{r})H_y(\mathbf{r}), \tag{15}$$

where

$$\mathbf{T}_h(\mathbf{r}) = \begin{pmatrix} A(\mathbf{r}) \\ B(\mathbf{r}) \end{pmatrix}$$

is the vertical transfer function or the tipper (Vozoff 1972). Substituting (14) and (15) into (13) yields

$$\begin{aligned} &\left[\frac{\partial Z_{yx}(\mathbf{r})}{\partial x} - \frac{\partial Z_{xx}(\mathbf{r})}{\partial y}\right] H_x(\mathbf{r}) + \left[\frac{\partial Z_{yy}(\mathbf{r})}{\partial x} - \frac{\partial Z_{xy}(\mathbf{r})}{\partial y}\right] H_y(\mathbf{r}) \\ &\quad + \left[Z_{yx}(\mathbf{r})\frac{\partial H_x(\mathbf{r})}{\partial x} - Z_{xx}(\mathbf{r})\frac{\partial H_x(\mathbf{r})}{\partial y}\right] \\ &\quad + \left[Z_{yy}(\mathbf{r})\frac{\partial H_y(\mathbf{r})}{\partial x} - Z_{xy}(\mathbf{r})\frac{\partial H_y(\mathbf{r})}{\partial y}\right] \\ &= -i\omega\mu_0[A(\mathbf{r})H_x(\mathbf{r}) + B(\mathbf{r})H_y(\mathbf{r})]. \end{aligned} \tag{16}$$

The left-hand side of (16) involves the MT impedance and horizontal magnetic components and their horizontal gradients. The horizontal magnetic component anomaly at each site can be expressed by the horizontal geomagnetic transfer function $V(\mathbf{r})$ as

$$\begin{aligned} \mathbf{H}_h(\mathbf{r}) &= V(\mathbf{r})\mathbf{H}_h(\mathbf{r}_0) \\ &= \begin{pmatrix} V_{xx}(\mathbf{r}) & V_{xy}(\mathbf{r}) \\ V_{yx}(\mathbf{r}) & V_{yy}(\mathbf{r}) \end{pmatrix} \begin{pmatrix} H_x(\mathbf{r}_0) \\ H_y(\mathbf{r}_0) \end{pmatrix}, \end{aligned} \tag{17}$$

where $\mathbf{r}_0$ stands for a reference site. Horizontal gradients of the horizontal magnetic components in (16) can then be written in terms of horizontal gradients of the horizontal transfer functions, e.g.

$$\begin{aligned} \frac{\partial H_x(\mathbf{r})}{\partial x} &= \left[\frac{\partial}{\partial x}(V_{xx}(\mathbf{r}), V_{xy}(\mathbf{r}))\right] \begin{pmatrix} H_x(\mathbf{r}_0) \\ H_y(\mathbf{r}_0) \end{pmatrix} \\ &= \left[\frac{\partial}{\partial x}(V_{xx}(\mathbf{r}), V_{xy}(\mathbf{r}))\right] V^{-1}(\mathbf{r}) \begin{pmatrix} H_x(\mathbf{r}) \\ H_y(\mathbf{r}) \end{pmatrix}, \end{aligned} \tag{18}$$

where V^{-1} denotes the inverse of V. Thus, (16) results in an expression that relates the vertical transfer function to the MT impedance and horizontal gradients of the impedance and horizontal transfer functions.

The electromagnetic fields observed with an ideal site distribution should satisfy the vertical component of Faraday's law (16). However, in actual experiments, the finite difference approximation of the horizontal gradients of the electric field often yields large errors, as shown in Fig. 2, because the actual site distribution is too sparse to describe the field variations due to small scattering bodies. Removal of this error is possible either by spatial filtering (Torres-Verdin & Bostick 1992) or by measuring a long-line electric field (Uyeshima *et al.* 1999). Of course, one can obtain a data set that is perfectly consistent with Faraday's law by performing an infinitely dense MT survey. In such a case, a solution can be found that explains all the features of the response functions, although the modelling

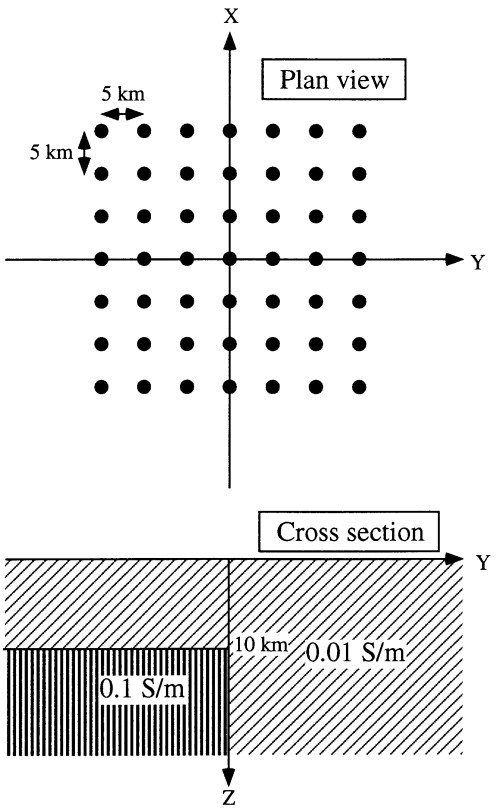

Figure 3. The 2-D electrical model used in the first test of the decomposition. Black dots in the plan view are observation sites where synthetic EM responses are calculated.

capability may remain a problem. The necessity of removing galvanic distortions arises only when the site spacing is insufficient to describe the spatial features of the galvanic scattered fields. On the other hand, this indicates that such a measurement will be able to estimate accurately the finite difference of the horizontal gradients of the undistorted regional electric field, provided that the site spacing is sufficiently small for this purpose. Therefore, the observed data should be consistent with Faraday's law, if the impedance tensor in (16) is replaced by the undistorted impedance tensor

$$Z_{\mathrm{U}}(\mathbf{r}) = C^{-1}(\mathbf{r}) Z_{\mathrm{D}}(\mathbf{r}), \tag{19}$$

where C^{-1} denotes the inverse of C.

By applying field data to the identity (16), the distortion tensor or its inverse at each observation site $\mathbf{r}_i$ can be determined so as to minimize the objective function Q_1:

$$Q_1 = \sum_i \| \nabla \times [C^{-1}(\mathbf{r}_i)\mathbf{E}(\mathbf{r}_i)]|_z - [-i\omega\mu_0 H_z(\mathbf{r}_i)] \|^2, \tag{20}$$

where $\| \cdot \|^2$ is the two-norm. Alternatively, the object function may be expressed as

$$Q_1 = \sum_i \| \mathbf{T}_{\mathrm{h}}^{\mathrm{cal}}(\mathbf{r}_i) - \mathbf{T}_{\mathrm{h}}^{\mathrm{obs}}(\mathbf{r}_i) \|^2, \tag{21}$$

where $\mathbf{T}_{\mathrm{h}}^{\mathrm{cal}}(\mathbf{r}_i)$ and $\mathbf{T}_{\mathrm{h}}^{\mathrm{obs}}(\mathbf{r}_i)$ are the calculated and observed vertical transfer functions, respectively. From the expressions of (16), (18) and (19), it is seen that $\mathbf{T}_{\mathrm{h}}^{\mathrm{cal}}(\mathbf{r}_i)$ is composed of the inverse of the distortion tensor $C^{-1}(\mathbf{r}_i)$, the observed MT impedance tensor $Z_{\mathrm{D}}(\mathbf{r}_i)$, and the horizontal gradients of the impedance and horizontal transfer functions. Thus, the

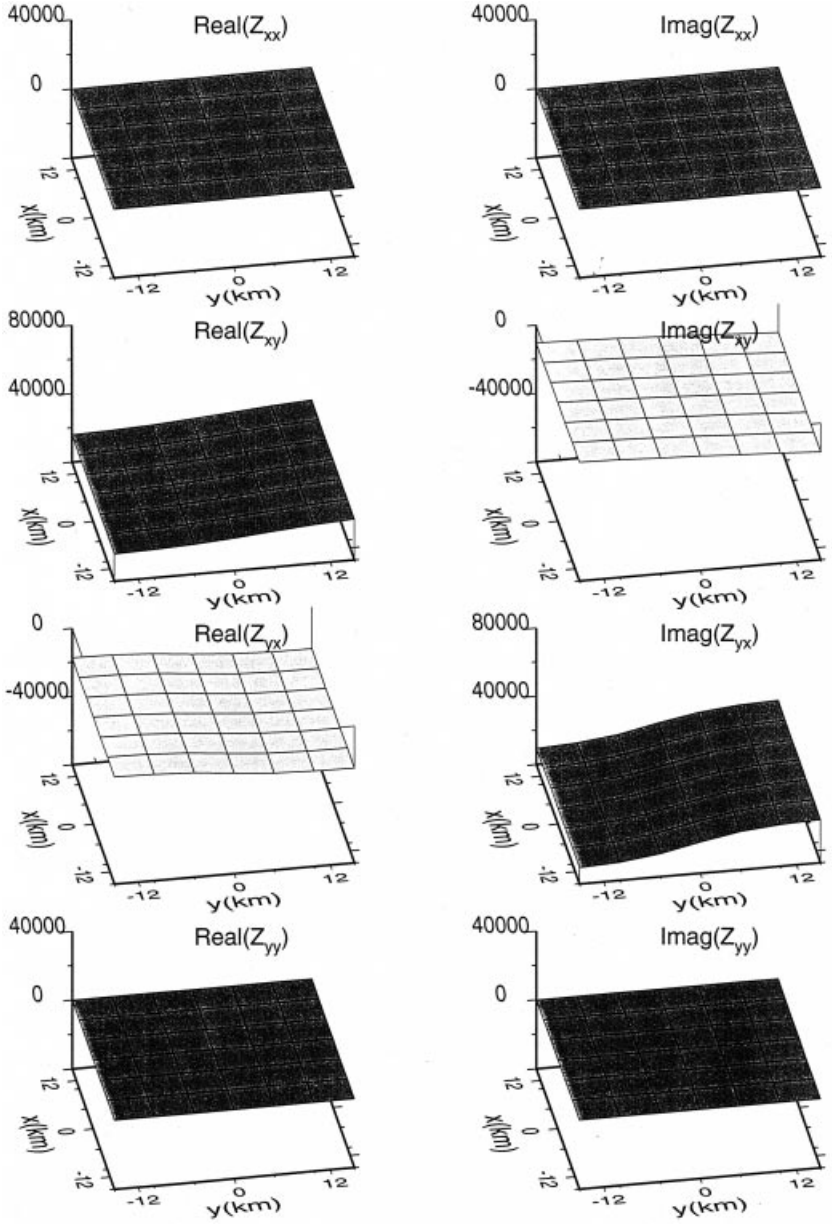

Figure 4. Real and imaginary components of the 2-D undistorted MT impedance tensor at a period of 100 s. Each element of the impedance is plotted with dark and light shading corresponding to positive and negative values, respectively. Each impedance value is normalized by $i\omega\mu_0$.

equation inside the norm in (20) contains four degrees of freedom at each site, thereby enabling us to determine $C^{-1}(\mathbf{r}_i)$ uniquely using the observed data. In actual practice, the frequency dependence of C^{-1} must be penalized to produce a stable solution.

FORWARD MODELLING

In the previous section, we proposed a method to remove galvanic distortion from the observed MT impedance. In this section, the result of a numerical experiment using forward modelling will be described in order to examine the method's performance. For simplicity and comparison, first we present an example with 2-D regional structure that has previously been studied in other works. The result of 3-D modelling will then be shown for a simple case with a regional 3-D conductivity heterogeneity.

Fig. 3 shows the model of regional 2-D geoelectric structure to be considered. The strike direction was taken as coinciding with the X-direction. The finite difference method (FDM) was employed to solve the frequency-domain induction equation in 2-D space (Smith & Booker 1991) for three periods: 80, 100 and 120 s, and the EM responses were calculated at each observation point and distributed with 5 km spacing, whereas the horizontal grid spacing of the model is 1 km. Since there is no near-surface heterogeneity to cause galvanic distortion in the model, the calculated vertical magnetic components and finite difference approximations of the electric field rotation are consistent with Faraday's law due to smooth lateral variations of the regional electromagnetic field. The resulting spatial distribution of the MT impedance is shown in Fig. 4 for a period of 100 s. Since the structure is purely 2-D, only off-diagonal elements of the impedance tensor take non-zero values, with a smooth lateral variation only in the Y-direction.

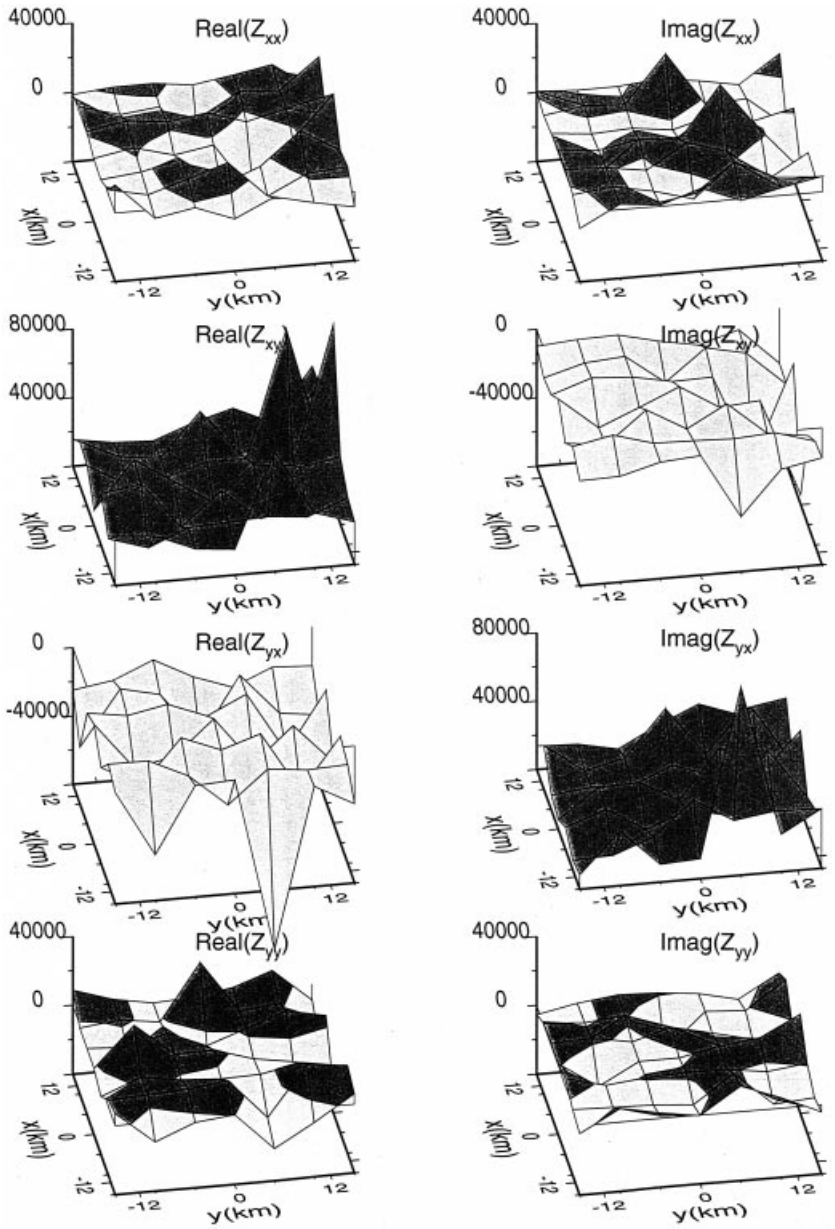

Figure 5. Real and imaginary components of the distorted MT impedance tensor calculated from the impedance elements in Fig. 4.

Galvanic distortion was randomly assigned to the impedance tensor at each observation site using the expression of Groom & Bailey (1991):

$$C = gTSA, \tag{22}$$

where g is a scalar parameter for the static shift, and T, S and A are the twist, shear and anisotropy tensors, respectively. The distortion tensor C was assumed to be constant for the narrow frequency band of present interest. A random number was assigned to each of the scalar parameters and elements of operators in (22) at each site. The resulting synthetic data were heavily distorted (Fig. 5).

Using calculated vertical and horizontal geomagnetic transfer functions, we determined the inverse of the distortion tensor by a finite difference Levenberg–Marquardt method to minimize the objective function (21), and obtained the undistorted MT impedance at each site as shown in Fig. 6. Comparing Fig. 6 with Fig. 4, a good agreement can be recognized between the values of Z_{xx} and Z_{xy}, whilst a large discrepancy exists in the distributions of Z_{yx} and Z_{yy}. In other words, the present scheme can recover the E-polarization but not the H-polarization responses. As will be shown below, however, this result is quite natural given the assumption of a purely 2-D regional structure.

As is well known, the electromagnetic fields in 2-D induction decouple into two modes, the E-polarization and H-polarization modes. Field gradients exist only in the direction perpendicular to the electric field in the E-polarization, while they exist only parallel to the electric field in the H-polarization. The present method constrains the impedance relation by use of

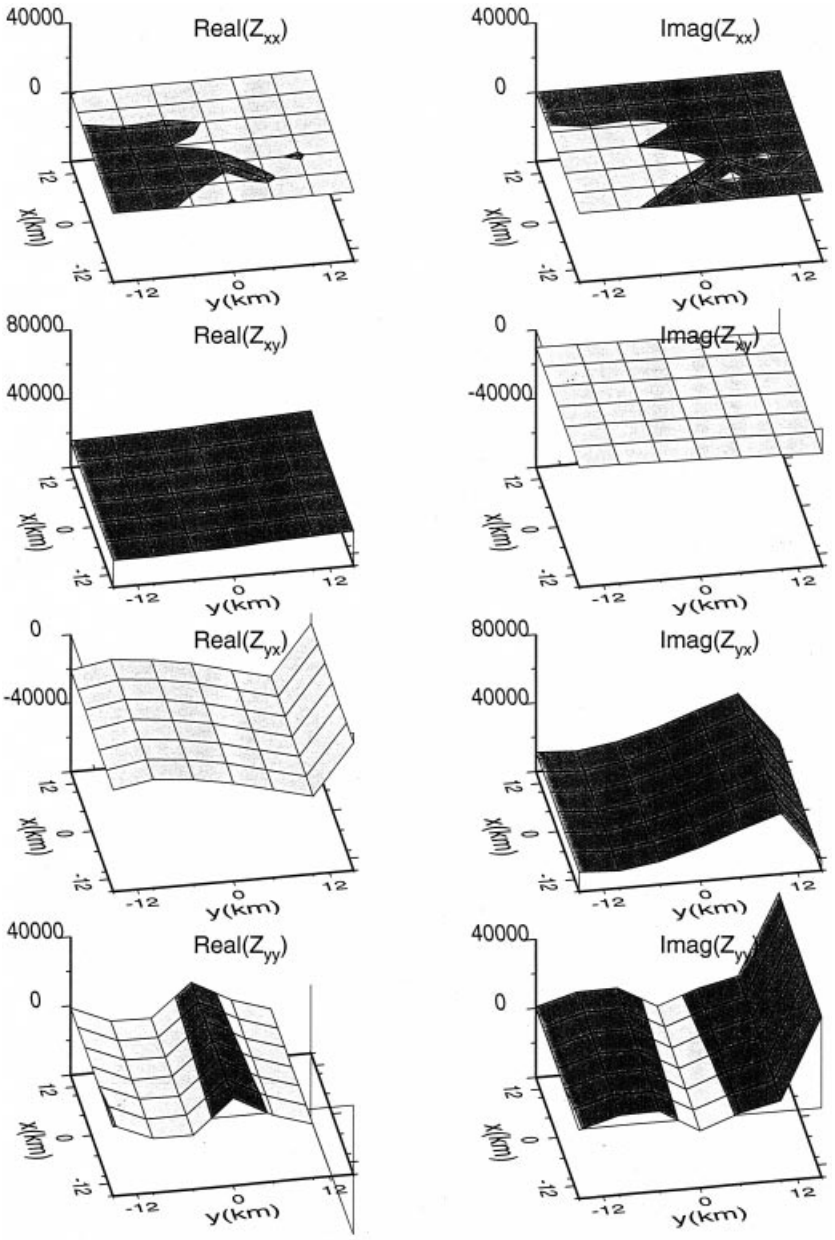

Figure 6. Real and imaginary components of the decomposed MT impedance tensor recovered by minimizing the objective function Q_1. Note the good agreement with Fig. 4 for Z_{xx} and Z_{xy}.

a rotation operation on the electric field, as shown in (13), and this operator consists only of spatial derivatives in the direction perpendicular to the electric field. Consequently, this mathematical condition cannot constrain the H-polarization electromagnetic field at all. The unsuccessful decomposition of H-polarization impedance elements can be simply ascribed to a decoupling of the two modes in 2-D induction, as will be discussed in the following section.

Although this would not seem to be a serious problem so far as general 3-D structures are concerned, it would be better to present a possible solution for recovering the undistorted H-polarization impedance in the case of 2-D structures. The discussion in the above paragraph indicates that this problem might be overcome by introducing mathematical constraints involving spatial derivatives along the electric field direction. One possible way to introduce such constraints is by means of the conservation law of the current density,

$$\nabla \cdot \mathbf{j} = 0, \tag{23}$$

which involves such spatial derivatives and could provide an additional mathematical condition to constrain the impedance. However, it is impossible to apply this condition directly to the observed data, because this condition includes the vertical gradient of j_z, which is not usually measured in an MT survey. Thus the gradient $\partial j_z / \partial z$ must be evaluated numerically with an appropriate model. In this paper, an iterative procedure combined with inversion is proposed as a means of determining the distortion tensor. The exact formulation is not shown here, but will be given in a later paper (Munekane & Utada 2000, in preparation).

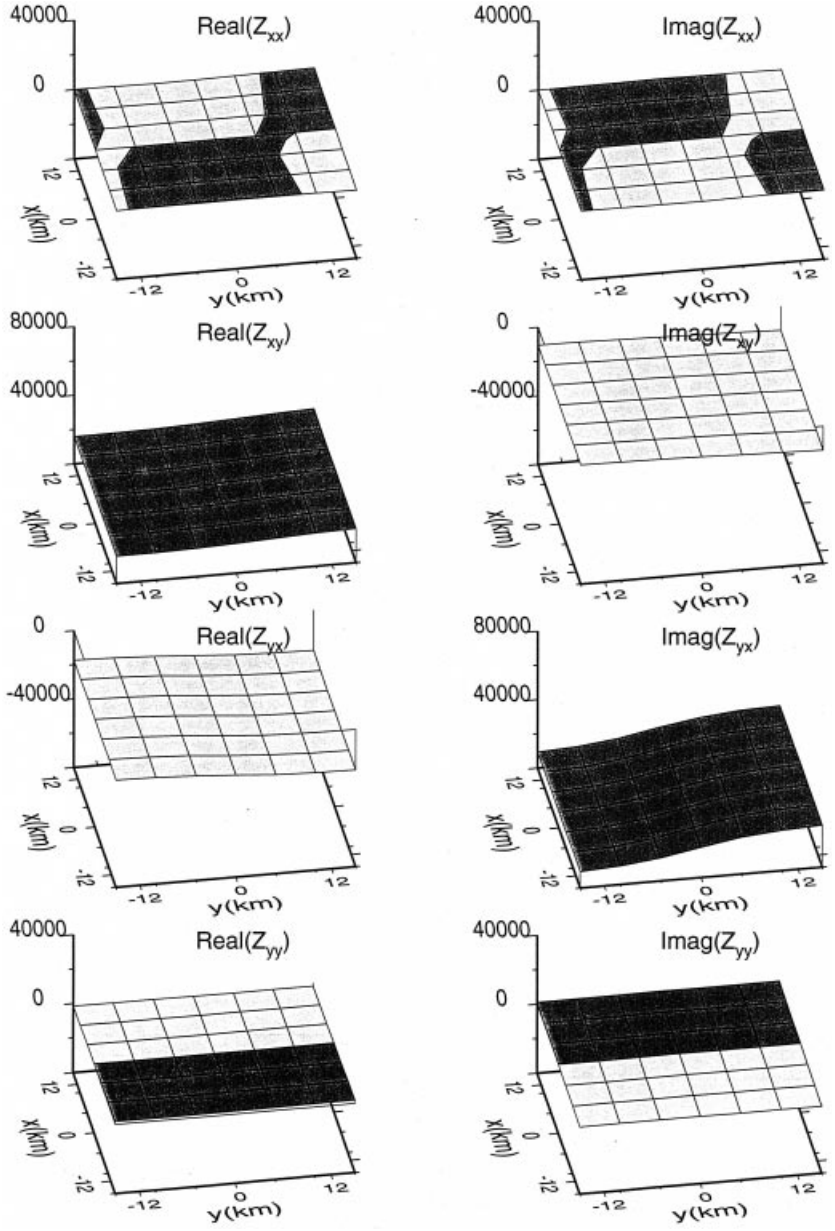

Figure 7. Real and imaginary components of the decomposed MT impedance tensor by minimizing the objective function $Q_1 + Q_2$. Note improved agreement with Fig. 4.

Fig. 7 shows the distribution of the undistorted impedance tensor elements obtained by using the inverse of the distortion tensor determined by simultaneously minimizing

$$Q_2 = \sum_i \left\| \frac{\partial[\sigma(Z_{xx}H_x + Z_{xy}H_y)]}{\partial x} + \frac{\partial[\sigma(Z_{yx}H_x + Z_{yy}H_y)]}{\partial y} + \frac{\partial j_z}{\partial z} \right\|^2 \quad (24)$$

and Q_1 (see 21), that is, minimizing the objective function $Q_1 + Q_2$. In this example, $\partial j_z/\partial z$ values calculated in the forward modelling were used to evaluate the objective function Q_2. Few discrepancies can be recognized between the responses in Fig. 7 and those in Fig. 4. The forward modelling was made for periods of 10 to 1000 s, but no significant difference was observed, as shown in Fig. 8, in which the root mean square misfit rms is defined as

$$\text{rms} = \left[\frac{1}{N} \sum_{i=1}^{N} \frac{\sum_{j,k=x,y} |Z_{jk}^{\text{cal}}(\mathbf{r}_i) - Z_{jk}^{0}(\mathbf{r}_i)|^2}{\sum_{j,k=x,y} |Z_{jk}^{0}(\mathbf{r}_i)|^2} \right]^{1/2}, \quad (25)$$

where $Z_{jk}^{0}(\mathbf{r}_i)$ denotes the undistorted impedance element and $Z_{jk}^{\text{cal}}(\mathbf{r}_i)$ is either the distorted or the decomposed impedance element at a site $\mathbf{r}_i$.

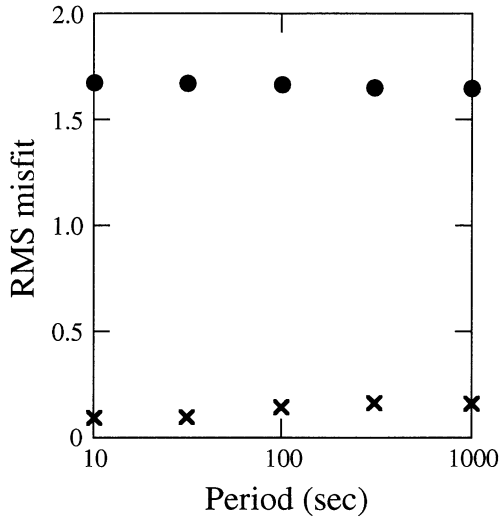

Figure 8. Rms misfits between elements of the distorted and undistorted impedance tensor (black dots) and between elements of the decomposed and undistorted impedance tensor (crosses). Misfits are partly due to numerical errors and to site spacing five times greater than the computational grid spacing. Calculations were performed for five periods: 10, 30, 100, 300 and 1000 s.

The next numerical result shows that the present decomposition scheme is applicable for an actual 3-D case. Synthetic data were calculated for a period of 40 s at sites over a conducting body embedded in a homogeneous half-space (Fig. 9) using the 3-D algorithm of Mackie *et al.* (1993). In the same procedure as in the 2-D case, the synthetic distorted impedances were decomposed by minimizing the object function Q_1 in (20). Figs 10, 11 and 12 show spatial distributions of synthetic impedance elements for the undistorted, distorted and decomposed impedances, respectively. Note that the vertical axis is exaggerated in Figs 10 and 12 to show lateral variations more clearly. Decomposition reduced the rms misfit from 2.87 to 0.074 in this case.

DISCUSSION

The 2-D forward modelling results shown in the previous section should be useful in clarifying our understanding of the proposed method. The method is intended to be applied to a general 3-D regional structure, in which the electromagnetic fields may not be decoupled into independent modes. In the 3-D case, it is convenient to represent each component of the electromagnetic fields consisting of poloidal magnetic (PM) and toroidal magnetic (TM) modes, as can often be seen in the theory of EM induction in a horizontally stratified conducting medium with a spatially non-uniform source field (Chave & Luther 1990). Such an expression can be found more often in global induction studies (Schultz & Zhang 1994). Thus, the undistorted field $\mathbf{E}_{\text{U}}(\mathbf{r})$ in (8) may be rewritten as

$$\mathbf{E}_{\text{U}} = \mathbf{E}_{\text{PM}}(\mathbf{r}) + \mathbf{E}_{\text{TM}}(\mathbf{r}) . \quad (26)$$

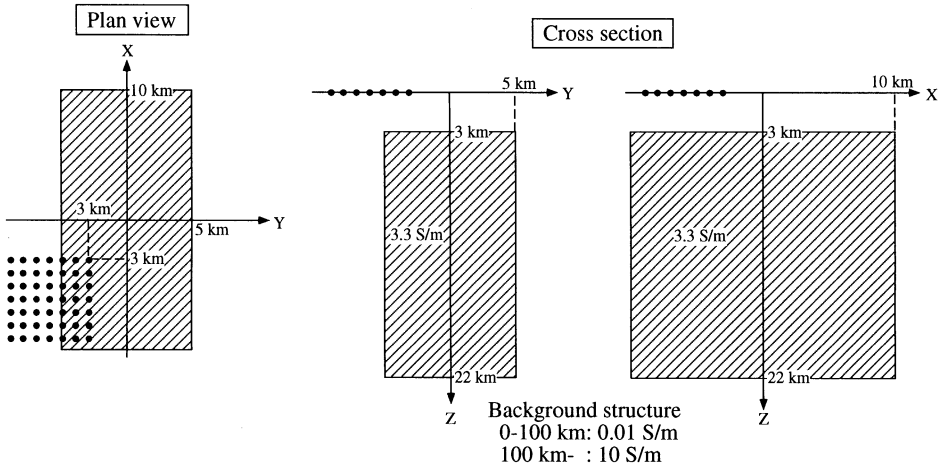

Figure 9. The 3-D electrical model used to test the decomposition scheme. EM responses are calculated at the observation sites shown by black dots.

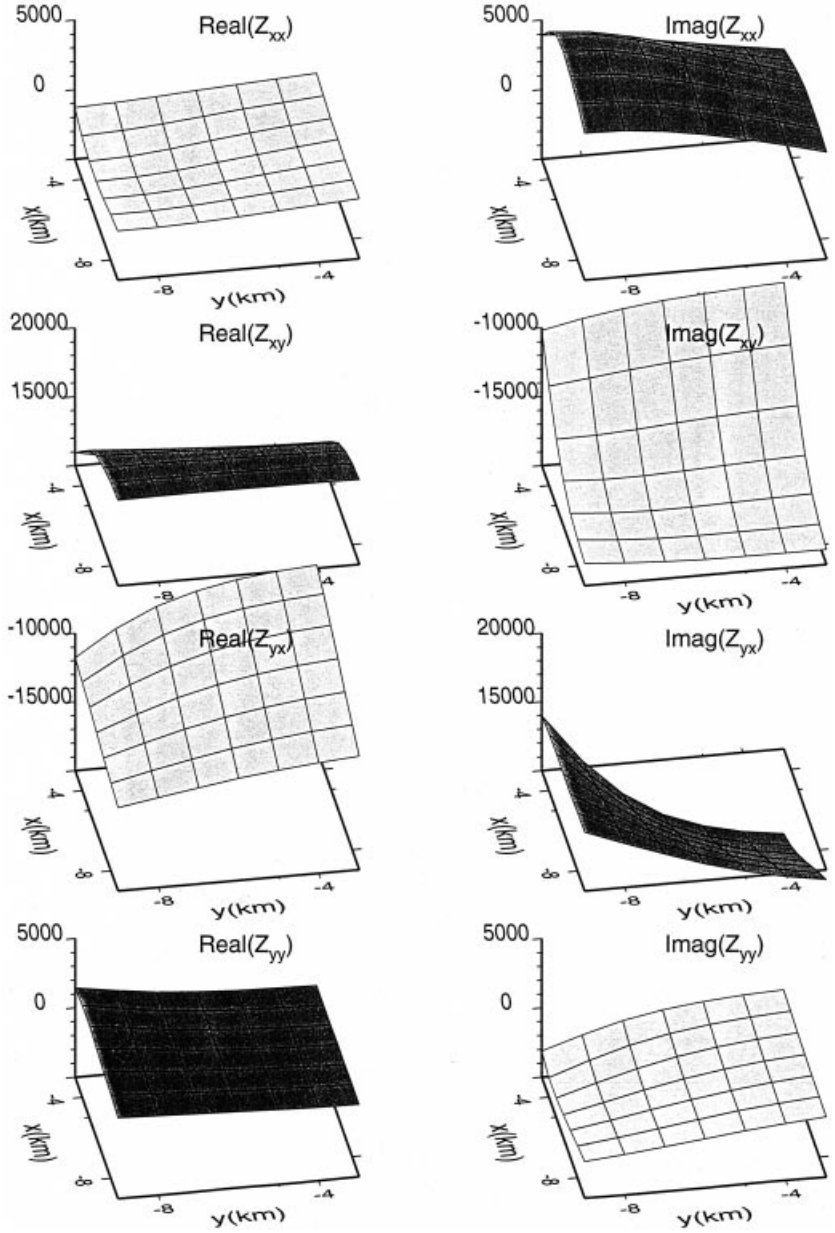

Figure 10. Real and imaginary components of the 3-D undistorted MT impedance tensor calculated from the model shown in Fig. 9 at a period of 40 s. Note that all components are non-zero due to 3-D induction.

Since the TM mode does not have a vertical magnetic component at the surface, the vertical component of Faraday's law,

$$\nabla \times \mathbf{E}_{\mathrm{TM}}(\mathbf{r})|_z = 0\,, \tag{27}$$

is automatically satisfied for this mode. This indicates that the present method uses only the consistency of the PM mode with Faraday's law to determine the distortion tensor. Because the PM and TM modes are always coupled in a 3-D situation, a qualitative consideration predicts that a problem of indefinite TM mode decomposition does not occur in the general case. The 3-D modelling result in the previous section has shown an example supporting this prediction with a simple case study. More detailed 3-D forward modelling studies will be made in a later paper (Munekane & Utada 2000, in preparation), which should provide useful information for the application of this method to field data.

More field efforts are required to apply this method to actual data, because the method requires 2-D spatial derivatives of the EM response functions in order to remove galvanic distortions. It is obvious that all elements of the response functions must be accurately estimated, and thus that the use of a highly reliable method for time series analysis will be indispensable. In addition to being highly accurate estimates, all the EM responses must be obtained in a 2-D array with appropriate spacing. Accordingly, we are currently conducting an experiment in which the present method will be applied to the study of the electrical conductivity distribution beneath a

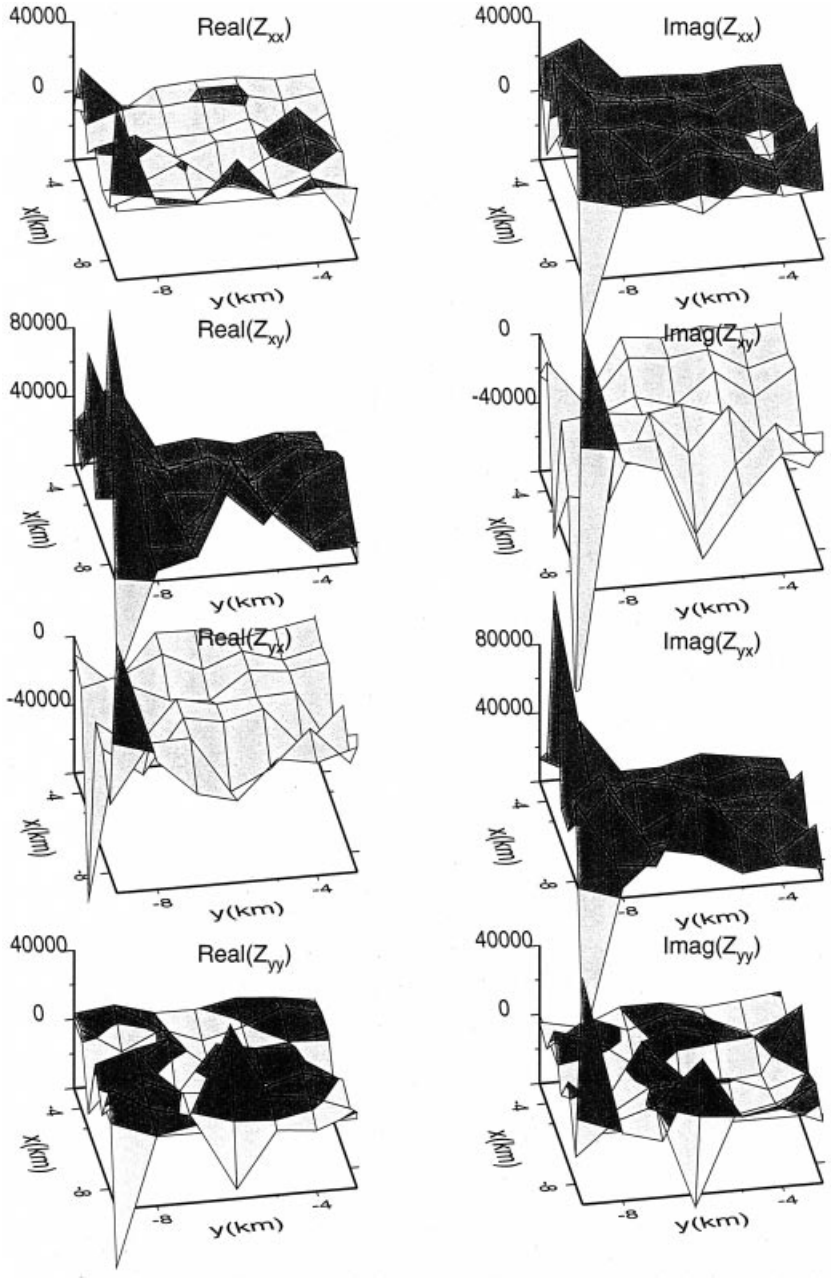

Figure 11. Real and imaginary components of the distorted MT impedance tensor calculated from the impedance elements in Fig. 10.

volcanic area in Japan (Munekane *et al.* 1998). However, there are few previous field examples to which the present method can be fully applied; in many cases this is because the horizontal transfer functions were not obtained, even though the MT impedance and vertical transfer function were obtained in a 2-D array (e.g. Takasugi *et al.* 1992).

A slight simplification of the mathematical constraints (16) by neglecting gradients of the horizontal magnetic fields may be useful to widen the applicability of the method and also to clarify its physical meaning. This corresponds to the assumption of a uniform horizontal magnetic field, which may be acceptable in many cases. Neglecting the horizontal gradients in (16) gives

$$A(\mathbf{r}) = \frac{-1}{i\omega\mu_0}\left[\frac{\partial Z_{yx}(\mathbf{r})}{\partial x} - \frac{\partial Z_{xx}(\mathbf{r})}{\partial y}\right], \tag{28}$$

$$B(\mathbf{r}) = \frac{-1}{i\omega\mu_0}\left[\frac{\partial Z_{yy}(\mathbf{r})}{\partial x} - \frac{\partial Z_{xy}(\mathbf{r})}{\partial y}\right]. \tag{29}$$

We see from these two equations that the vertical transfer function can be expressed by the horizontal gradients of the MT impedance. In other words, these gradients give an explicit expression of the well-known nature of induction arrows that point to the conducting side when there is a horizontal variation

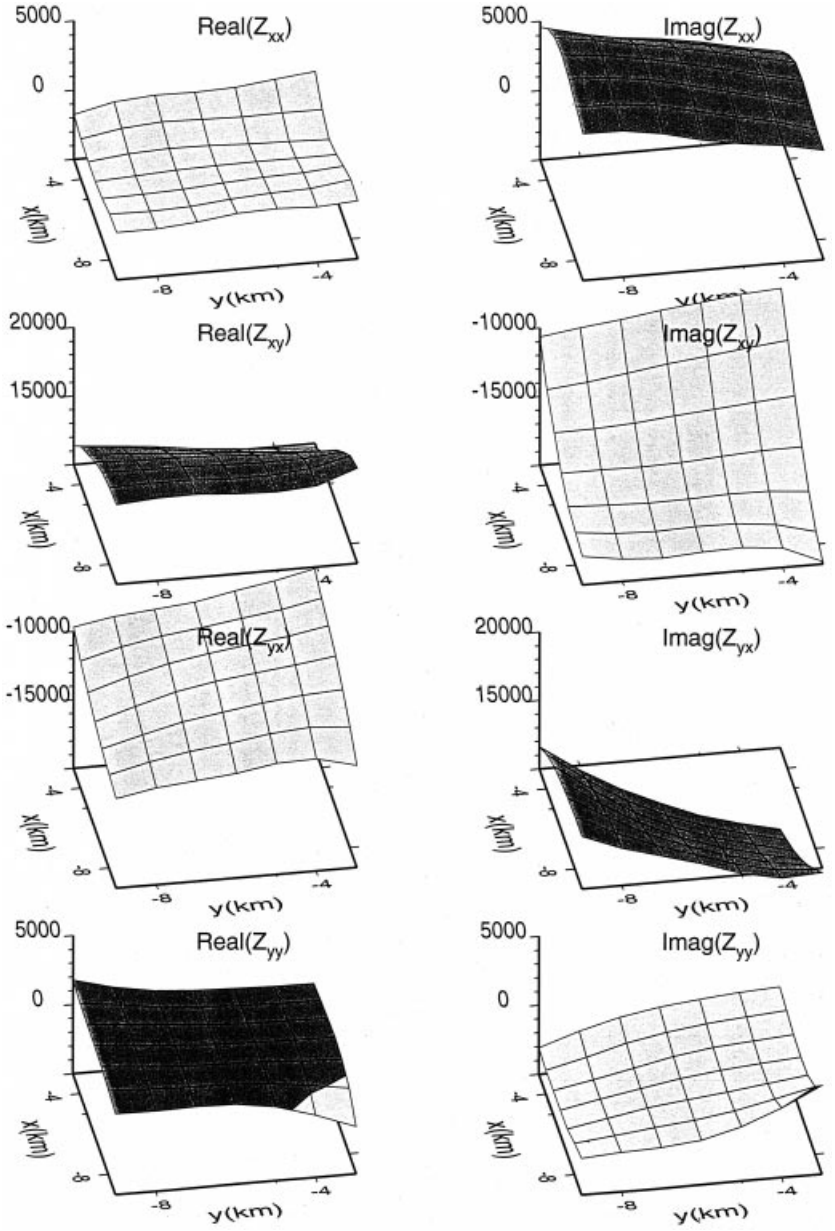

Figure 12. Real and imaginary components of the MT impedance tensor recovered by the decomposition technique. Note the good agreement with Fig. 10.

of electrical conductivity structure (Parkinson 1962; Vozoff 1972). In magnetovariational (MV) studies, subsurface conductivity structures are investigated by means of this property of the induction arrows (e.g. Porath & Dziewonski 1971; Cerv *et al.* 1997). It is easy to derive the linear relation between the transfer function and MT impedance given by Zhang *et al.* (1993) using a linear approximation of the horizontal gradients in (28) and (29).

When the horizontal magnetic components are assumed to be laterally uniform, decomposition of the MT impedance can be performed based on the constraints (28) and (29); that is, determining the distortion tensor by matching the horizontal gradients of the MT impedance with the vertical transfer function at each site. However, it should be noted that this simplification results in a distortion tensor that is non-unique. The absolute value of each impedance element cannot be constrained, because the impedance values themselves do not appear—rather only their spatial gradients appear—in (28) and (29). As a result, any combination of impedance elements that satisfies (28) and (29) can be a solution. When this simplification is applied, each of four impedance elements must be fixed for at least one site in order to control the absolute value. It may be possible to choose the least distorted site as a reference. However, the static shift parameter will still remain undetermined, but should be obtainable by any of a number of approaches proposed to date (e.g. Sternberg *et al.* 1988; Jones 1988; Bahr 1991; Ogawa & Uchida 1996).

Although it is most appropriate to apply the present method to a situation with severe 3-D induction effects, there may still exist some advantage in applying it to a case where the regional structure is nearly 2-D. This is because the present method with constraints (16) completely recovers the undistorted

E-polarization impedance including static shift and thus the regional strike direction. This information should help to reduce the number of unknowns in actual interpretations of MT data.

As pointed out in an earlier section, MT data collection must be performed with an optimum site spacing in order to describe the spatial features of the inductive electromagnetic fields and thereby fully apply the present method. This indicates that appropriate site spacing depends on the frequency of interest. If MT surveys are performed with wide-band instruments, as they often have been in recent years, site spacing must be optimized at the highest observation frequency. Optimized at lower frequencies, responses at higher frequencies will suffer from not only galvanic but also magnetic (inductive) distortions, which prevents a simple treatment of the distortion tensor.

This study, therefore, recommends that the design of MT surveys be made in several narrow frequency bands (each covering two decades or so of frequency) with different site spacings optimized for each band, although, of course, a wide-band survey in a wide area with fine site spacing is ideal. Once MT data are collected at a certain observation band $\lambda_0 > \lambda > \lambda_1$ [see (5) for a definition of the inductive scale length λ] with optimal site spacing, galvanic distortion can be removed by using the present method. The resulting undistorted impedance will reflect a conductivity distribution of the Earth that is composed of a 3-D regional structure covered by a thin layer (thickness l) with a smoothly changing conductance (Fig. 13). Measurements at a higher frequency band ($\lambda_1 > \lambda > \lambda_2$) are necessary for resolving smaller structures within the thin layer. The observation band must be chosen so that λ is comparable with the layer thickness l. The site distribution must be much denser because the scale of the target structure is smaller.

Throughout this paper, the distortion tensor C has been assumed to be a second-order real tensor, which means that all distortion effects are of purely galvanic origin. This is not a physical requirement, and therefore extension of the theory to a case where the tensor C is complex is possible in principle. This corresponds to a situation in which inductive scattered components are not negligible in the distorted field, or in other words, magnetic distortion exists. Thus it is indicated that a problem of magnetic distortion decomposition can be solved by simply letting the distortion tensor be complex in the present approach. Although there remains a practical problem of how to determine the second-order complex tensor C, this approach may solve the problem in determining the magnetic distortion tensor D (Chave & Smith 1994).

CONCLUSIONS

This paper re-examined the physics governing the effects of near-surface small conductivity inhomogeneities on the electromagnetic field variations, and presented a new idea for removing galvanic distortions of the MT impedance in cases where the regional structure is 3-D. Derivation of the mathematical conditions necessary to determine the distortion tensor was based on the simple electromagnetic theory represented in Faraday's law. The physics of galvanic distortions were clarified through the derivation. A forward modelling with a regional 2-D/3-D structure with 3-D galvanic distortions implied the potential applicability of this method to some extent. However, only a simple case was considered in this study. Further detailed numerical experiments in 3-D situations will be needed to verify the efficiency and limitations of the present method.

ACKNOWLEDGMENTS

We wish to thank Igor Rokityansky, Dmitry Avdeev, Yoichi Sasai, Arvidas Cheryauka, Tsuneomi Kagiyama, Makoto Uyeshima, Yasuo Ogawa and Hisayoshi Shimizu for fruitful discussions. Comments by Alan Chave, Gary McNeice and Martyn Unsworth were helpful in improving the manuscript. This work was partly supported by the Ministry of Education, Science, Sports and Culture, Japan (grant-in-aid 9640504).

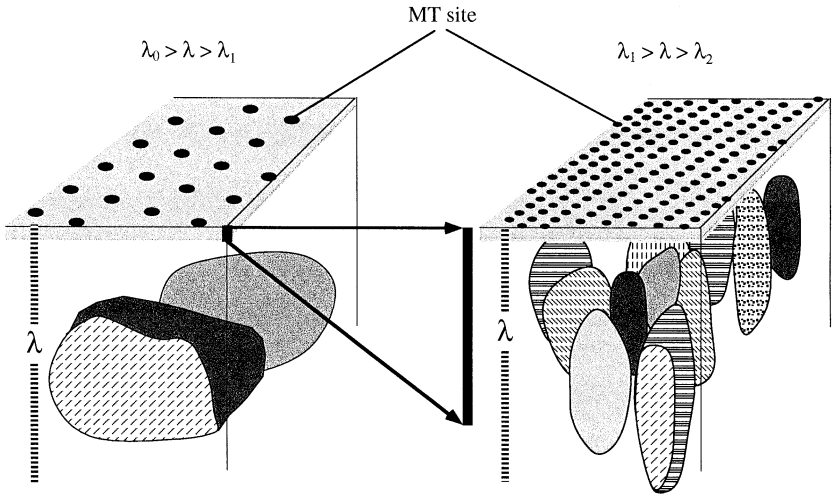

Figure 13. Schematic diagram of the field design recommended by the present study. Black dots represent the MT observation sites. Left and right diagrams show optimal site distributions for the lower and higher frequency bands, respectively. Each frequency band is indicated by the inductive scale length λ (left: $\lambda_0 > \lambda > \lambda_1$; right $\lambda_1 > \lambda > \lambda_2$), which is shown by a thick dotted bar in each diagram. In each frequency band, the present method removes galvanic distortion due to the near-surface inhomogeneities. The surface structure can then be replaced by a thin layer with smoothly changing conductance. Note that the thickness of the thin layer l for the lower band becomes of a regional scale (comparable with λ) for the higher band, as indicated by the thick solid bar.

REFERENCES

Avdeev, D.B., Kuvshinov, A.V., Pankratov, O.V. & Newman, G.A., 1997. High-performance three-dimensional electromagnetic modelling using Modified Neumann Series. Wide-band numerical solution and examples, *J. Geomag. Geoelectr.,* **49,** 1519–1540.

Bahr, K., 1988. Interpretation of the magnetotelluric impedance tensor: regional induction and local telluric distortion, *J. Geophys.,* **62,** 119–127.

Bahr, K., 1991. Geological noise in magnetotelluric data: a classification of distortion types, *Phys. Earth planet Inter.,* **66,** 24–38.

Cerv, V., Kovatikova, S., Pek, J., Pecova, J. & Praus, O., 1997. Model of electrical conductivity distribution across central Europe, *J. Geomag. Geoelectr.,* **47,** 1585–1600.

Chave, A.D. & Luther, D.S., 1990. Low frequency, motionally induced electromagnetic fields in the ocean, 1: Theory, *J. geophys. Res.,* **95,** 7185–7200.

Chave, A.D. & Smith, J.T., 1994. On electric and magnetic galvanic distortion tensor decompositions, *J. Geophys. Res.,* **99,** 4669–4682.

Groom, R.W. & Bahr, K., 1992. Corrections for near surface effects: decomposition of the magnetotelluric impedance tensor and scaling corrections for regional resistivities: a tutorial, *Surv. Geophys.,* **13,** 341–379.

Groom, R.W. & Bailey, R.C., 1989. Decomposition of magnetotelluric impedance tensors in the presence of local three-dimensional galvanic distortion, *J. geophys. Res.,* **94,** 1913–1925.

Groom, R.W. & Bailey, R.C., 1991. Analytic investigations of the effects of near-surface three-dimensional galvanic distortion, *Geophysics,* **56,** 496–518.

Hohmann, G.W., 1975. Three-dimensional induced polarization and electromagnetic modelling, *Geophysics,* **40,** 309–324.

Jiracek, G.R., 1990. Near-surface and topographic distortions in electromagnetic induction, *Surv. Geophys.,* **11,** 163–203.

Jones, A.G., 1988. Static shift of magnetotelluric data and its removal in a sedimentary basin environment, *Geophysics,* **53,** 967–978.

Mackie, R.L., Madden, T.R. & Wannamaker, P.E., 1993. Three-dimensional electromagnetic modeling using difference equations—theory and comparisons to integral equation solutions, *Geophysics,* **58,** 215–226.

Munekane, H., Kagiyama, T. & Utada, H., 1998. The resistivity structure in the southern Kyushu area, *EOS, Trans. Am. geophys. Un.,* **79,** W106.

Ogawa, Y. & Uchida, T., 1996. A two-dimensional magnetotelluric inversion assuming Gaussian static shift, *Geophys. J. Int.,* **126,** 69–76.

Parkinson, W.D., 1962. The influence of continents and oceans on geomagnetic variations, *Geophys. J. R. astr. Soc.,* **4,** 441–449.

Pedersen, L.B. & Rasmussen, T.M., 1985. Inversion of magnetotelluric data: a non-linear approach, *Geophys. Prospect.,* **37,** 669–695.

Porath, H. & Dziewonski, A., 1971. Crustal electrical conductivity anomalies in the Great Plains Province of the United States, *Geophysics,* **36,** 382–395.

Schultz, A. & Zhang, T.S., 1994. Regularized spherical harmonic analysis and the three dimensional electromagnetic response of the earth, *Geophys. J. Int.,* **116,** 141–156.

Smith, J.T., 1995. Understanding telluric distortion matrices, *Geophys. J. Int.,* **122,** 219–226.

Smith, J.T., 1997. Estimating galvanic-distortion magnetic fields in magnetotellurics, *Geophys. J. Int.,* **130,** 65–72.

Smith, J.T. & Booker, J.R., 1991. Rapid inversion of two- and three-dimensional magnetotelluric data, *J. geophys. Res.,* **96,** 3905–3922.

Sternberg, B.K., Washburne, J.C. & Pellerin, L., 1988. Correction for the static shift in magnetotellurics using transient electromagnetic soundings, *Geophysics,* **53,** 1459–1468.

Takasugi, S., Tanaka, K., Kawamaki, N. & Muramatsu, S., 1992. High spatial resolution of the resistivity structure revealed by a dense network MT measurement—a case study in the Minamikayabe area, Hokkaido, Japan, *J. Geomag. Geoelectr.,* **44,** 289–308.

Torres-Verdin, C. & Bostick, F.X., Jr., 1992. Principles of spatial electric field filtering in magnetotellurics: electromagnetic array profiling (EMAP), *Geophysics,* **57,** 603–622.

Uchida, T., 1993. Smooth 2-D inversion for magnetotelluric data based on statistical criterion ABIC, *J. Geomag. Geoelectr.,* **45,** 841–858.

Uyeshima, M., Utada, H. & Nishida, Y., 1999. Network-MT method and its first results in the central and eastern part of Hokkaido, northern Japan, *Phys. Earth planet. Inter.,* in press.

Vozoff, K., 1972. The magnetotelluric method in the exploration of sedimentary basins, *Geophysics,* **37,** 98–114.

Zhang, P., Pedersen, L.B., Mareschal, M. & Chouteau, M., 1993. Channelling contribution to tipper vectors: a magnetic equivalent to electrical distortion, *Geophys. J. Int.,* **113,** 693–700.

Zhdanov, M.S. & Fang, S., 1996. Quasi linear approximation in 3-D electromagnetic modeling, *Geophysics,* **61,** 646–665.